EFFICIENT NONLINEAR FILTER STABILIZATION OF THE LERAY-α MODEL

AZIZ TAKHIROV * AND CATALIN TRENCHEA †

Abstract. In this work we study a novel adaptive nonlinear filtering applied to the Leray-α model. Unlike its classical counterpart, the new filtering requires the solution of a linear elliptic problem, with constant coefficients, at each time step. The action of the adaptive nonlinear filter throughout the integration time is refactorized as the solution of a linear system, with the same matrix and multiple right hand-sides. We discuss the theoretical properties of the new filtering approach applied to the BDF2 approximation of the Leray-α model. Numerical tests demonstrate that the filtering damps the high wave number modes of the solution and has similar level of accuracy with the classical filter. Some benchmark results are also presented.

1. Introduction. Many large eddy simulation (LES) turbulent models [1, 2, 3, 4, 5] seek to approximate suitable local averages of flow variables. The spatial averaging of a variable $\phi(x,t)$ is usually performed via a filtering procedure, with the paradigm being the convolution with the Gaussian kernel:

$$\overline{\phi}(x,t) := \int\limits_{\mathbb{R}^d} \frac{c}{\alpha^d} \exp\left(-\frac{|x-y|^2}{\alpha^2}\right) \phi(y,t)\, dy, \tag{1.1}$$

where $0 < \alpha \ll 1$ is the filtering radius, c is a normalization constant, $x, y \in \mathbb{R}^d$, and $d = 2, 3$ is the space dimension. For bounded domains $\Omega \subset \mathbb{R}^d$, the differential filter of Germano [6] (also called the Helmholtz filter) is often viewed as a correct extension of the Gaussian filter:

$$\begin{aligned} -\alpha^2 \Delta \overline{u} + \overline{u} + \nabla \lambda &= u \text{ in } \Omega, \\ \nabla \cdot \overline{u} &= 0 \text{ in } \Omega, \\ \overline{u} &= u \text{ on } \partial\Omega. \end{aligned} \tag{1.2}$$

In any turbulence model, the purpose of filtering, such as in (1.1) or (1.2), is to truncate the high-frequency modes of the flow velocity u, both in physical and spectral spaces, which is a highly nonlinear process. However, the linear filtering (1.2) truncates scales uniformly in space, thereby over-regularizing the laminar parts of the solution and often removing critical flow structures [7, 8, 9]. This shortcoming was recognized in [10], where a nonlinear, adaptive spatial filter was proposed:

$$\begin{aligned} -\alpha^2 \nabla \cdot (a(u,p,f) \nabla \overline{u}) + \overline{u} + \nabla \lambda &= u, \\ \nabla \cdot \overline{u} &= 0, \end{aligned} \tag{1.3}$$

where $a(\cdot)$ satisfies, for β some small constant that enforces positivity,

$$\begin{aligned} &0 < \beta \leq a(\cdot) \leq 1 \text{ for any } (x,t), \\ &a(\cdot) \simeq 0 \text{ selects regions requiring no local filtering,} \\ &a(\cdot) \simeq 1 \text{ selects regions requiring } O(\alpha) \text{ local filtering.} \end{aligned} \tag{1.4}$$

The nonlinear adaptive filtering was synthesized with the evolve-filter-relax based stabilization in [10, 11] and with the Leray-α model in [12, 13]. It was mostly tested with academic problems, with the notable exception being the FDA Nozzle benchmark of [14].

Even though (1.3) is a linear system of equations, it requires a matrix to be assembled at each time step, and the solution of a mixed problem. It is often the case that the flow solvers are based on projection-type schemes, where one avoids a solution of the mixed problem via

* Department of Mathematics, University of Sharjah, UAE. email: atakhirov@sharjah.ac.ae.
† Department of Mathematics, University of Pittsburgh, USA. email: trenchea@pitt.edu.

relaxing the incompressibility constraint. Thus, the development of such filtering systems that share this property deserves attention.

Such filtering schemes were considered in [15, 16], where first and second order artificial compressibility based nonlinear filtering were proposed and studied. Specifically, the filtering in [16] was demonstrated to be overall second order, but only as a part of evolve-filter-relax based stabilization scheme. Its second order extension to other models, such as Leray-α [17, 18], the approximate-deconvolution model [19] or the Bardina scale similarity model [20], is not obvious without increased computational complexity.

These observations have led us to consider in Section 2.3 a new formulation of the nonlinear spatial filter (1.3). The filter is based on ideas from [15, 16], the innovation being that it uses the same matrix for the solution of the linear elliptic equation, at every step during the time integration.

For clarity of exposition, we will develop our adaptive nonlinear filtering algorithm for the Leray-α model [18]:

$$\begin{aligned} u_t + \overline{u}\cdot\nabla u + \nabla p - \nu\Delta u &= f, \\ \nabla\cdot u &= 0, \end{aligned}$$

where now $\overline{u}$ solves the new filtering equation.

We have opted for the Leray model solely for the simplicity of its implementation. As it is well-known, it directly regularizes the convective term by reducing its degrees of freedom and satisfies the same energy equation as the Navier-Stokes equation (NSE). The initial simulations of a mixing layer [7, 8] were reported to be very promising; however the tests on wall-bounded flows in [21] produced unsatisfactory results. It was advocated in [22] to blend the Leray-α model with an eddy-viscosity model to obtain results that match the experimental data well. It should be noted that all the preceding references in this paragraph are performed with the classical Helmholtz filter (1.2).

The paper is organized as follows. In Section 2 we introduce the notation, the choice of an indicator function, present our numerical algorithm and state the desired properties of the new adaptive filtering step. In Section 3 we prove that our algorithm satisfies the required properties. Namely, we establish the stability of the filtering step, prove its second-order accuracy (for a filtering radius of the order of the time-step), and provide estimates for the error between the solution of the NSE and the solution to our algorithm. We dedicate Section 4 to numerical tests, and draw some conclusions in the last Section.

2. Preliminaries.

2.1. Notations. We denote by $\Omega\subset\mathbb{R}^d$ an open, simply connected domain with piecewise smooth boundary Γ. The $L^2(\Omega)$ norm and inner product will be denoted by $\|\cdot\|$ and $(\cdot,\cdot)$. For simplicity of presentation, we assume a no-slip boundary condition. In this setting, the appropriate velocity and pressure spaces are defined as

$$X := (H_0^1(\Omega))^d,\ Q := L_0^2(\Omega).$$

We use as the norm on X , $\|v\|_X := \|\nabla v\|_{L^2(\Omega)}$. The space of divergence-free (solenoidal) functions, and the weighted $\mathrm{H}_{\gamma,\mathrm{div}}$ space are given by

$$\begin{aligned} V &:= \{v\in X:\ (\nabla\cdot v, q) = 0\ \ \forall q\in Q\} \\ \mathrm{H}_{\gamma,\mathrm{div}} &:= \left\{v\in L^2(\Omega)^d : \|v\|_{\mathrm{H}_{\alpha,\mathrm{div}}} := \sqrt{\|v\|^2+\gamma\|\nabla\cdot v\|^2} < \infty\right\}, \end{aligned}$$

respectively, where $\gamma>0$ is an arbitrary constant.

We will study flow problems in the space-time $\Omega\times[0,T]$ cylinder domain. For a fixed timestep τ, we set $N=[T/\tau]$. For a given sequence of functions $\{\phi^n\}_{n=1}^N\subset X$, an indicator function $0\le a(\cdot)\le 1$, and for any $w\in X$ we define the following quantities

$$\|\nabla w\|_{a^n} := \|\sqrt{a(\phi^n)}\nabla w\|,\quad \|\Delta_{a^n} w\|_* := \sup_{v\in X}\frac{(a(\phi^n)\nabla w,\nabla v)}{\|v\|},\quad 1\le n\le N,$$

and

$$H_N^*(\Omega) := \{w \in X : \|\Delta_{a^n} w\|_* < \infty\}, \quad 1 \le n \le N.$$

We also define the discrete L^p-norms with $p = 2$ or ∞

$$\|w\|_{L^2(0,T,H^*)} = \left(\tau \sum_{n=1}^{N} \|\Delta_{a^n} w^n\|_*^2\right)^{1/2}, \quad \|w\|_{L^2(0,T,\mathrm{H}_{\gamma,\mathrm{div}})} = \left(\tau \sum_{n=1}^{N} \|w^n\|_{\mathrm{H}_{\gamma,\mathrm{div}}}^2\right)^{1/2},$$
$$\|w\|_{L^\infty(0,T,X)} = \max_{1\le n\le N} \|w^n\|_X,$$

where $w = (w^1, w^2, \cdots, w^N)$. For $\tau = 1$ the discrete norms correspond to the ℓ^p-norms on $(H^*)^N, \mathrm{H}_{\gamma,\mathrm{div}}^N, X^N$.

2.2. Indicator functions. For theoretical and computational reasons, the indicator function $a(u, p, f)$ must be constructed so that it satisfies (1.4). Several indicator functions have been proposed in the literature. A number of phenomenology-based indicator functions were listed in [10], while in [15] an energy residual (entropy) based indicator function inspired by [23, 24] was considered. Another family of indicator functions based on approximate deconvolution operators was studied in [13], which we adopt in this paper:

$$a(u) = \frac{|u - \overline{u}_H|}{\max\left(\|u - \overline{u}_H\|_{L^\infty(\Omega)}, 1\right)},$$

where $\overline{u}$ is the Helmholtz filter of u without the enforcement of mass conservation:

$$\begin{aligned} -\alpha^2 \Delta \overline{u}_H + \overline{u}_H &= u \text{ in } \Omega, \\ \overline{u}_H &= u \text{ on } \partial\Omega. \end{aligned} \tag{2.1}$$

2.3. Numerical algorithm. The two key properties [3, pg. 14] of any reasonable spatial filter are:

(1) $\overline{w} \to w$ in some reasonable norm as $\delta \to 0$;
(2) norm of $\overline{w}$ is uniformly controlled by the norm of w.

We also want the filtering to have the following properties:

(3) time-independent matrix;
(4) avoid solving a mixed problem;
(5) be second-order (consistent) accurate in time.

The filter considered in [15, 16]

$$\begin{aligned} -\delta^2 \Delta\left(\overline{w^{n+1}} - \overline{w^n}\right) + \overline{w^{n+1}} + \nabla\lambda^{n+1} - \delta^2 \nabla\cdot(a(w^{n+1})\nabla\overline{w^n}) &= w^{n+1}, \\ \lambda^{n+1} - \lambda^n + \nabla\cdot\overline{w^{n+1}} &= 0, \end{aligned} \tag{2.2}$$

meets all the criteria except the last one: the divergence is only first order accurate. While higher order extensions of the artificial compressibility scheme have been proposed [25, 26], they all have increased computational complexity. On the other hand, a non-solenoidal advecting velocity field is known to produce a non-physical result. E.g., as shown in [21], it can give rise to spurious production of turbulent kinetic energy very close to the wall, which degrades the performance of the Leray-α model.

Herein we opted to enforce (approximate) incompressibility via bootstrapping:

ALGORITHM 2.1. *Given a forcing $f \in L^\infty(0,T;H^{-1}(\Omega))$, an initial velocity u_0, a timestep $\tau > 0$, filter radius δ, endtime T, $w^{n+1} := 2u^n - u^{n-1}$, $\gamma \ge \chi > 0$ and integer N satisfying $T = N\tau$, find (u^{n+1}, p^{n+1}) such that*

$$\begin{aligned} \textbf{\textit{Filter:}} \quad & -\delta^2\Delta\left(\overline{w^{n+1}} - \overline{w^n}\right) + \overline{w^{n+1}} - \gamma\nabla\nabla\cdot\overline{w^{n+1}} - \delta^2\nabla\cdot(a(w^{n+1})\nabla\overline{w^n}) \\ & = w^{n+1} - \chi\nabla\nabla\cdot w^{n+1}, \end{aligned} \tag{2.3}$$

Evolve:
$$\frac{3u^{n+1}-4u^n+u^{n-1}}{2\tau}+\big(\overline{w^{n+1}}\cdot\nabla\big)u^{n+1}+\nabla p^{n+1}-\nu\Delta u^{n+1}=f(t^{n+1}), \quad (2.4)$$
$$\nabla\cdot u^{n+1}=0. \quad (2.5)$$

REMARK 2.2. *The grad-div operator $-\gamma\nabla\nabla\cdot$ frequently occurs in numerical schemes for incompressible flows. For larger values of γ, the linear system arising from (2.3) is more accurate and ill-conditioned at the same time. However, due to the adapted right hand side $-\chi\nabla\nabla\cdot$, cf. [27, 28], the conditioning of the linear system could have a favorable dependence on γ. Namely, when $\gamma>\chi\gg 1$ and $a(\cdot)\simeq 0$, we show in Section 3 that the condition number is dominated by $\mathcal{O}(\gamma/\chi)$ on shape-regular family of meshes. The numerical tests in Section 4 also demonstrate the $\mathcal{O}(\gamma/\chi)$ dependence even when $a(\cdot)\neq 0$. On the other hand, even a slight increase in the value of γ/χ was observed to significantly improve the mass conservation.*

3. Theoretical results. We start by examining the 'filter' step (2.3) separately from the time-stepping procedure described in the 'evolve' step (2.4)-(2.5). In order to do this, let us consider two given arbitrary sequences

$$(\phi^1,\dots,\phi^N)\in X^N,\qquad (\mathrm{w}^0,\mathrm{w}^1,\dots,\mathrm{w}^N)\in X^{N+1}, \quad (3.1)$$

and a function $\mathrm{w}:[0,T]\times\Omega\to\mathbb{R}^d$, such that for all $t\in[0,T],\mathrm{w}(t,\cdot)\in X$, which also interpolates the sequence $\{\mathrm{w}^n\}_{n=0}^N$, i.e.,

$$\mathrm{w}(t^n,\cdot)=\mathrm{w}^n,\qquad \forall\, n=0,1,\cdots,N. \quad (3.2)$$

We now denote by $(\overline{\mathrm{w}^1},\dots,\overline{\mathrm{w}^N})$ the sequence generated by the general 'filter' step in Algorithm 2.1, with indicator functions $a(\phi^{n+1})$ instead of $a(\mathrm{w}^{n+1})$, namely

$$\begin{aligned}&-\delta^2\Delta\left(\overline{\mathrm{w}^{n+1}}-\overline{\mathrm{w}^n}\right)+\overline{\mathrm{w}^{n+1}}-\gamma\nabla\nabla\cdot\overline{\mathrm{w}^{n+1}}-\delta^2\nabla\cdot(a(\phi^{n+1})\nabla\overline{\mathrm{w}^n}) \quad (3.3)\\ &=\mathrm{w}^{n+1}-\chi\nabla\nabla\cdot\mathrm{w}^{n+1}.\end{aligned}$$

First we note that (3.3) can be written as

$$\begin{aligned}&\overline{\mathrm{w}^{n+1}}-\delta^2\nabla\cdot(a(\phi^{n+1})\nabla\overline{\mathrm{w}^{n+1}})-\delta^2\nabla\cdot\Big(\big(1-a(\phi^{n+1})\big)\nabla(\overline{\mathrm{w}^{n+1}}-\overline{\mathrm{w}^n})\Big)-\gamma\nabla\nabla\cdot\overline{\mathrm{w}^{n+1}}\\ &=\mathrm{w}(t^{n+1})-\chi\nabla\nabla\cdot\mathrm{w}(t^{n+1}), \quad (3.4)\end{aligned}$$

where in the right hand side we have used (3.2).
To better understand the behavior of the filter step (3.3), we borrow an interpretation from backward error analysis and geometric integration, based on the notion of modified equations (see e.g. [29, 30, 31, 32, 33, 34] and the references therein). Let us consider now two smooth functions $\overline{\mathrm{w}}:\Omega\times[0,T]$ and $\overline{\mathrm{w}}:\Omega\times[0,T]$ which satisfy the following equations

$$\overline{\mathrm{w}}-\delta^2\nabla\cdot\big(a(\mathrm{w})\nabla\overline{\mathrm{w}}\big)-\gamma\nabla\nabla\cdot\overline{\mathrm{w}}=\mathrm{w}-\chi\nabla\nabla\cdot\mathrm{w}, \quad (3.5)$$

and respectively

$$\overline{\mathrm{w}}-\delta^2\nabla\cdot\big(a(\mathrm{w})\nabla\overline{\mathrm{w}}\big)-\gamma\nabla\nabla\cdot\overline{\mathrm{w}}-\delta^2\tau\nabla\cdot\Big(\big(1-a(\mathrm{w})\big)\nabla\overline{\mathrm{w}}_t\Big)=\mathrm{w}-\chi\nabla\nabla\cdot\mathrm{w}. \quad (3.6)$$

We remark that (3.5) is similar to the nonlinear adaptive filter equation (1.3), while (3.6) is an $\mathcal{O}(\tau)$ perturbation of (3.5), called a modified equation to (3.5). From (3.4) it follows that the (3.3) filtered values $\{\overline{\mathrm{w}}^n\}_{n=1}^N$ are closer to the manifold $\overline{\mathrm{w}}(t)$ than to $\overline{\mathrm{w}}(t)$:

$$\overline{\mathrm{w}}^n-\overline{\mathrm{w}}(t^n)=\mathcal{O}(\tau),\qquad \overline{\mathrm{w}}^n-\overline{\mathrm{w}}(t^n)=\mathcal{O}(\tau^2).$$

This observation allows us to interpret the actions of the Helmholtz filter (1.3) and the new filter (3.3) on the given sequence $\{w^n\}_{n=0}^N$ by examining the energy balance for the manifolds $\overline{\mathrm{w}}(t)$ and $\overline{\overline{\mathrm{w}}}(t)$. Namely, while (1.3), (3.5) generate $\mathcal{O}(\delta^2)$-dissipation in the rough regions $a(\cdot) \approx 1$, the new filter (3.3), (3.6) also creates an $\mathcal{O}(\delta^2\tau)$ term related to time-changes in the enstrophy in the smooth regions $a(\cdot) \approx 0$:

$$\begin{aligned}&\|\overline{\mathrm{w}}\|^2 + 2\delta^2\|\sqrt{a(\mathrm{w})}\nabla\overline{\mathrm{w}}\|^2 + (2\gamma-\chi)\|\nabla\cdot\overline{\mathrm{w}}\|^2 + \delta^2\tau\int_\Omega \big(1-a(\mathrm{w})\big)\frac{\partial}{\partial t}\big|\nabla\overline{\mathrm{w}}\big|^2 dx\\ &= \|\mathrm{w}\|^2 + \chi\|\nabla\cdot\mathrm{w}\|^2 - \|\overline{\mathrm{w}}-\mathrm{w}\|^2 - \chi\|\nabla\cdot(\overline{\mathrm{w}}-\mathrm{w})\|^2.\end{aligned}$$

We point out that (3.3) can be written as

$$\begin{aligned}&\big(I-\delta^2\Delta-\gamma\nabla\nabla\cdot\big)\overline{\mathrm{w}^{n+1}}\\ &= \big(I-\delta^2\Delta-\beta\nabla\nabla\cdot\big)\mathrm{w}^{n+1} + \delta^2\Delta(\mathrm{w}^{n+1}-\overline{\mathrm{w}^n}) + \delta^2\nabla\cdot\big(a(\phi^{n+1})\nabla\overline{\mathrm{w}^n}\big),\end{aligned}$$

which shows that the new filtering requires only one time independent matrix assembly, i.e., it satisfies the key property (3). This enables the refactorization of the nonlinear filter (2.3), throughout the whole numerical integration, as the resolution of a linear system with multiple right hand-sides.
Moreover, we can view the error between the filtered and non-filtered values as

$$\begin{aligned}&\overline{\mathrm{w}^{n+1}} - \mathrm{w}^{n+1}\\ &= \big(I-\delta^2\Delta-\gamma\nabla\nabla\cdot\big)^{-1}\Big((\gamma-\chi)\nabla\nabla\cdot\mathrm{w}^{n+1} + \delta^2\Delta(\mathrm{w}^{n+1}-\overline{\mathrm{w}^n}) + \delta^2\nabla\cdot\big(a(\mathrm{w}^{n+1})\nabla\overline{\mathrm{w}^n}\big)\Big),\end{aligned}$$

where $J_{\delta^2} := \big(I-\delta^2\Delta-\gamma\nabla\nabla\cdot\big)^{-1}$ is the resolvent [35, page 182] of the maximal monotone operator $-\big(\Delta+\frac{\gamma}{\delta^2}\nabla\nabla\cdot\big)$.

3.1. Properties of the filter. We first prove that the modified nonlinear filter (3.3) satisfies property (2), i.e., the filtered values $\{\overline{\mathrm{w}^n}\}$ are bounded above by the non-filtered values $\{\mathrm{w}^n\}$.

LEMMA 3.1. *The filtered values* $\{\overline{\mathrm{w}}^n\}$ *satisfy*

$$\{\overline{\mathrm{w}^n}\} \in \ell^\infty(0,T,X)\cap\ell^2(0,T,\mathrm{H}_{\gamma,\mathrm{div}})$$

and the following estimate holds

$$\begin{aligned}&\delta^2\big\|\nabla\overline{\mathrm{w}^N}\big\|^2 + \sum_{n=0}^{N-1}\|\overline{\mathrm{w}^{n+1}}\|^2_{\mathrm{H}_{\gamma,\mathrm{div}}}\\ &\quad+(\gamma-\chi)\sum_{n=0}^{N-1}\|\nabla\cdot\overline{\mathrm{w}^{n+1}}\|^2 + \sum_{n=0}^{N-1}\|\mathrm{w}^{n+1}-\overline{\mathrm{w}^{n+1}}\|^2_{\mathrm{H}_{\chi,\mathrm{div}}}\\ &\quad+\delta^2\sum_{n=0}^{N-1}\big\|\sqrt{1-a(\phi^{n+1})}\nabla(\overline{\mathrm{w}^{n+1}}-\overline{\mathrm{w}^n})\big\|^2 + \delta^2\sum_{n=0}^{N-1}\Big(\big\|\nabla\overline{\mathrm{w}^{n+1}}\big\|^2_{a^{n+1}} + \big\|\nabla\overline{\mathrm{w}^n}\big\|^2_{a^{n+1}}\Big)\\ &= \delta^2\big\|\nabla\overline{\mathrm{w}^0}\big\|^2 + \sum_{n=0}^{N-1}\|\mathrm{w}^{n+1}\|^2_{\mathrm{H}_{\chi,\mathrm{div}}}.\end{aligned}\tag{3.7}$$

Moreover, if $\overline{\mathrm{w}^0}=0$ *then*

$$\|\overline{\mathrm{w}}\|_{\ell^2(0,T,\mathrm{H}_{\gamma,\mathrm{div}})} \le \|\mathrm{w}\|_{\ell^2(0,T,\mathrm{H}_{\chi,\mathrm{div}})}\tag{3.8}$$

$$(\mathrm{w},\overline{\mathrm{w}})_{\ell^2(0,T,\mathrm{H}_{\chi,\mathrm{div}})} \ge 0\tag{3.9}$$

and

$$(\mathrm{w} - \overline{\mathrm{w}}, \overline{\mathrm{w}})_{\ell^2(0,T,\mathrm{H}_{\chi,\mathrm{div}})} \geq 0. \tag{3.10}$$

Proof. We begin by testing (3.3) with $\overline{\mathrm{w}^{n+1}}$, which gives

$$\begin{aligned}\frac{\delta^2}{2}\left(\left\|\nabla\overline{\mathrm{w}^{n+1}}\right\|^2 - \left\|\nabla\overline{\mathrm{w}^{n}}\right\|^2 + \left\|\nabla(\overline{\mathrm{w}^{n+1}} - \overline{\mathrm{w}^{n}})\right\|^2\right) + \delta^2\left(a(\phi^{n+1})\nabla\overline{\mathrm{w}^{n+1}}, \nabla\overline{\mathrm{w}^{n}}\right)\\ + \|\overline{\mathrm{w}^{n+1}}\|^2_{\mathrm{H}_{\gamma,\mathrm{div}}} = \left(\mathrm{w}^{n+1}, \overline{\mathrm{w}^{n+1}}\right)_{\mathrm{H}_{\chi,\mathrm{div}}}.\end{aligned} \tag{3.11}$$

Applying the polarized identity

$$(a,b) = \frac{a^2 + b^2 - (a-b)^2}{2}$$

to the filtering term in (3.11) yields

$$\left(a(\phi^{n+1})\nabla\overline{\mathrm{w}^{n+1}}, \nabla\overline{\mathrm{w}^{n}}\right) = \frac{\left\|\nabla\overline{\mathrm{w}^{n+1}}\right\|^2_{a^{n+1}} + \left\|\nabla\overline{\mathrm{w}^{n}}\right\|^2_{a^{n+1}}}{2} - \frac{\left\|\nabla(\overline{\mathrm{w}^{n+1}} - \overline{\mathrm{w}^{n}})\right\|^2_{a^{n+1}}}{2}. \tag{3.12}$$

Then relation (3.12) allows us to rewrite (3.11) as

$$\begin{aligned}&\frac{\delta^2}{2}\left(\left\|\nabla\overline{\mathrm{w}^{n+1}}\right\|^2 - \left\|\nabla\overline{\mathrm{w}^{n}}\right\|^2\right) + \delta^2\frac{\left\|\sqrt{1-a(\phi^{n+1})}\nabla(\overline{\mathrm{w}^{n+1}} - \overline{\mathrm{w}^{n}})\right\|^2}{2}\\ &\quad + \frac{\delta^2}{2}\left(\left\|\nabla\overline{\mathrm{w}^{n+1}}\right\|^2_{a^{n+1}} + \left\|\nabla\overline{\mathrm{w}^{n}}\right\|^2_{a^{n+1}}\right) + \|\overline{\mathrm{w}^{n+1}}\|^2_{\mathrm{H}_{\gamma,\mathrm{div}}}\\ &= \left(\mathrm{w}^{n+1}, \overline{\mathrm{w}^{n+1}}\right)_{\mathrm{H}_{\chi,\mathrm{div}}}\\ &= \frac{1}{2}\|\mathrm{w}^{n+1}\|^2_{\mathrm{H}_{\chi,\mathrm{div}}} + \frac{1}{2}\|\overline{\mathrm{w}^{n+1}}\|^2_{\mathrm{H}_{\chi,\mathrm{div}}} - \frac{1}{2}\|\mathrm{w}^{n+1} - \overline{\mathrm{w}^{n+1}}\|^2_{\mathrm{H}_{\chi,\mathrm{div}}}.\end{aligned} \tag{3.13}$$

Summation over n from 0 to $N-1$ gives (3.7), and as a particular case, (3.8).

The inequality (3.9) is also immediately obtained by summation in (3.13). In order to derive the inequality (3.10), we can rewrite the equation (3.13) by moving $\|\overline{\mathrm{w}^{n+1}}\|^2_{\mathrm{H}_{\gamma,\mathrm{div}}}$ to the right hand side.

$$\begin{aligned}&\frac{\delta^2}{2}\left(\left\|\nabla\overline{\mathrm{w}^{n+1}}\right\|^2 - \left\|\nabla\overline{\mathrm{w}^{n}}\right\|^2\right) + \delta^2\frac{\left\|\sqrt{1-a(\phi^{n+1})}\nabla(\overline{\mathrm{w}^{n+1}} - \overline{\mathrm{w}^{n}})\right\|^2}{2}\\ &\quad + \frac{\delta^2}{2}\left(\left\|\nabla\overline{\mathrm{w}^{n+1}}\right\|^2_{a^{n+1}} + \left\|\nabla\overline{\mathrm{w}^{n}}\right\|^2_{a^{n+1}}\right)\\ &= \left(\mathrm{w}^{n+1} - \overline{\mathrm{w}^{n+1}}, \overline{\mathrm{w}^{n+1}}\right)_{\mathrm{H}_{\chi,\mathrm{div}}} - (\gamma - \chi)\|\nabla\cdot\overline{\mathrm{w}^{n+1}}\|^2.\end{aligned}$$

Summation over the time steps yields the remaining inequality. ∎

Next we quantify the error

$$\varepsilon^n := \mathrm{w}^n - \overline{\mathrm{w}^n}$$

in the proposed nonlinear filtering step. This corresponds to Theorem 2.5 from [10]. Assume that $\phi^1, \dots \phi^N$ and $\mathrm{w}^0, \mathrm{w}^1, \dots, \mathrm{w}^N$ satisfy (3.1), and moreover

$$\{\mathrm{w}^0, \mathrm{w}^1, \dots, \mathrm{w}^N\} \in \ell^2(H^2(\Omega)) \cap \ell^2(H^*_N(\Omega)). \tag{3.14}$$

We will prove that the errors made by the filtering procedure are second-order accurate.

LEMMA 3.2. *Under the assumptions (3.1) and (3.14), and if* $\overline{\mathrm{w}^0} = w^0$, *the errors* $\{\varepsilon^n\}_{n=1}^N$ *in the filtered values* $\{\overline{\mathrm{w}^n}\}_{n=1}^N$ *defined by (3.3) satisfy* $\{\varepsilon^n\}_{n=1}^N \in \ell^\infty(X)\cap\ell^2(\mathrm{H}_{\gamma,\mathrm{div}})$, *and the following estimates hold*

$$\begin{aligned}&\delta^2\left\|\nabla\varepsilon^N\right\|^2+\sum_{n=1}^N\|\varepsilon^n\|^2_{\mathrm{H}_{\gamma,\mathrm{div}}}\\&\leq 2\delta^4\tau\|\mathrm{w}_t\|^2_{L^2(0,T;H^2(\Omega))}+2\frac{\delta^4}{\tau}\|\mathrm{w}\|^2_{L^2(0,T;H^*(\Omega))}+\frac{(\gamma-\chi)^2}{\gamma\tau}\|\nabla\cdot\mathrm{w}\|^2_{L^2(0,T;L^2(\Omega))},\end{aligned}\tag{3.15}$$

and

$$\|\varepsilon\|_{L^2(0,T;\mathrm{H}_{\gamma,\mathrm{div}})}\leq C(\delta^2\tau+\delta^2)+\frac{\gamma-\chi}{\sqrt{\gamma}}\|\nabla\cdot\mathrm{w}\|_{L^2(0,T;L^2(\Omega))}.\tag{3.16}$$

In particular, for $\delta=\mathcal{O}(\tau)$ *and* $\nabla\cdot\mathrm{w}=\mathcal{O}(\tau^2)$, (3.16) *shows that the filter (3.3) satisfies property (5), i.e., is second-order accurate.*

Proof. Multiplying (3.3) by a test function $v\in X$, and subtracting both sides from

$$\delta^2\left(\nabla\left(\mathrm{w}^{n+1}-\mathrm{w}^n\right),\nabla v\right)+\delta^2\left(a(\phi^{n+1})\nabla\mathrm{w}^n,\nabla v\right)+\left(\mathrm{w}^{n+1},v\right)_{\mathrm{H}_{\gamma,\mathrm{div}}},$$

gives

$$\begin{aligned}&\delta^2\langle\nabla\left(\varepsilon^{n+1}-\varepsilon^n\right),\nabla v\rangle+\left(\varepsilon^{n+1},v\right)_{\mathrm{H}_{\gamma,\mathrm{div}}}+\delta^2\langle a(\phi^{n+1})\nabla\varepsilon^n,\nabla v\rangle\\&=\delta^2\left(\nabla\left(w^{n+1}-w^n\right),\nabla v\right)+\delta^2\left(a(\phi^{n+1})\nabla w^n,\nabla v\right)+(\gamma-\chi)\langle\nabla\cdot w^{n+1},\nabla\cdot v\rangle.\end{aligned}$$

Then picking $v=\varepsilon^{n+1}$ we arrive at the following estimate

$$\begin{aligned}&\frac{\delta^2}{2}\left(\left\|\nabla\varepsilon^{n+1}\right\|^2-\left\|\nabla\varepsilon^n\right\|^2\right)+\delta^2\frac{\left\|\sqrt{1-a(\phi^{n+1})}\nabla(\varepsilon^{n+1}-\varepsilon^n)\right\|^2}{2}\\&\quad+\frac{\delta^2}{2}\left(\left\|\nabla\varepsilon^{n+1}\right\|^2_{a^{n+1}}+\left\|\nabla\varepsilon^n\right\|^2_{a^{n+1}}\right)+\|\varepsilon^{n+1}\|^2_{\mathrm{H}_{\gamma,\mathrm{div}}}\\&=\delta^2\left(\nabla\left(\mathrm{w}^{n+1}-\mathrm{w}^n\right),\nabla\varepsilon^{n+1}\right)+\delta^2\left(a(\phi^{n+1})\nabla\mathrm{w}^n,\nabla\varepsilon^{n+1}\right)+(\gamma-\chi)\langle\nabla\cdot\mathrm{w}^{n+1},\nabla\cdot\varepsilon^{n+1}\rangle\\&\leq\frac{1}{2}\|\varepsilon^{n+1}\|^2_{\mathrm{H}_{\gamma,\mathrm{div}}}+\delta^4\left(\|\Delta(\mathrm{w}^{n+1}-\mathrm{w}^n)\|^2+\|\Delta_{a^{n+1}}\mathrm{w}^n\|^2_*\right)+\frac{(\gamma-\chi)^2}{2\gamma}\|\nabla\cdot\mathrm{w}^{n+1}\|^2.\end{aligned}\tag{3.17}$$

In the derivation of (3.17), we made use of a similar argument to one employed in (3.13). Summing over the time steps and using $\varepsilon^0=0$ and (3.2) completes the proof. ∎

3.2. Stability and error estimates. Using the G-stability of the BDF2 approximation [36, 37, 38], from (2.4)-(2.5) we obtain the following energy type equality

$$\begin{aligned}&\frac{1}{2}\|u^N\|^2+\frac{1}{2}\|2u^N-u^{N-1}\|^2+\frac{1}{2}\sum_{n=1}^{N-1}\|u^{n+1}+2u^n-u^{n-1}\|^2+\nu\tau\sum_{n=1}^{N-1}\|\nabla u^{n+1}\|^2\\&=\frac{1}{2}\|u^1\|^2+\frac{1}{2}\|2u^1-u^0\|^2+\frac{1}{2}\tau\sum_{n=1}^{N-1}\int_\Omega\nabla\cdot\overline{w^{n+1}}|u^{n+1}|^2.\end{aligned}$$

We now denote by

$$e^n(x)=u(t^n,x)-u^n(x)$$

the error between the solution of the Navier-Stokes equations and the solution of Algorithm 2.1. Subtracting from the Navier-Stokes equations evaluated at t^{n+1} the equations (2.4)-(2.5) we obtain

$$\frac{3e^{n+1}-4e^n+e^{n-1}}{2\tau}+u(t^{n+1})\cdot\nabla u(t^{n+1})-\left(\overline{w^{n+1}}\cdot\nabla\right)u^{n+1}+\nabla\left(p(t^{n+1})-p^{n+1}\right)-\nu\Delta e^{n+1}$$

$$= \frac{3u(t^{n+1}) - 4u(t^n) + u(t^{n-1})}{2\tau} - u_t(t^{n+1}),$$
$$\nabla \cdot \big(u(t^{n+1}) - u^{n+1}\big) = 0.$$

Using the definition of the filtering error ε^n and the choice of $w^{n+1} = 2u^n - u^{n-1}$ in Algorithm 2.1, the convection terms can be expressed equivalently by

$$\begin{aligned}
&\big(u(t^{n+1}) \cdot \nabla\big)u(t^{n+1}) - (\overline{w^{n+1}} \cdot \nabla)u^{n+1} \\
&= \big(e^{n+1} \cdot \nabla\big)u(t^{n+1}) + \big((u^{n+1} - 2u^n + u^{n-1}) \cdot \nabla\big)u(t^{n+1}) \\
&+ (\varepsilon^{n+1} \cdot \nabla)u(t^{n+1}) + \big(\overline{w^{n+1}} \cdot \nabla\big)e^{n+1}.
\end{aligned}$$

Therefore the error equation becomes

$$\begin{aligned}
&\frac{3e^{n+1} - 4e^n + e^{n-1}}{2\tau} + (e^{n+1} \cdot \nabla)u(t^{n+1}) + \big((u^{n+1} - 2u^n + u^{n-1}) \cdot \nabla\big)u(t^{n+1}) \\
&\quad + (\varepsilon^{n+1} \cdot \nabla)u(t^{n+1}) + (\overline{w^{n+1}} \cdot \nabla)e^{n+1} + \nabla\big(p(t^{n+1}) - p^{n+1}\big) - \nu\Delta e^{n+1} \\
&= \tau \int_{t^{n-1}}^{t^{n+1}} K_1(t)\frac{\partial^3}{\partial t^3}u(t)\,dt, \\
&\nabla \cdot e^{n+1} = 0,
\end{aligned} \tag{3.18}$$

where $K_1(t)$ is bounded by a constant independent of τ and u.

THEOREM 3.3. *Assume that the solution to the Navier-Stokes equations is smooth* $u \in L^\infty(0,T;W^{1,\infty}(\Omega)) \cap W^{3,2}(0,T;L^2(\Omega))$. *Then the errors in Algorithm 2.1 satisfy*

$$\begin{aligned}
&\frac{1}{2}\|e^N\|^2 + \frac{1}{2}\|2e^N - e^{N-1}\|^2 + \Big(\frac{1}{2} - \tau\Big)\sum_{n=1}^{N-1}\|e^{n+1} - 2e^n + e^{n-1}\|^2 + \nu\tau\sum_{n=1}^{N-1}\|\nabla e^{n+1}\|^2 \\
&\le \exp\Big(\tau\sum_{n=2}^{N}\frac{1 + C_\Omega\|u\|^2_{L^\infty(0,T;W^{1,\infty}(\Omega))}}{1 - \tau\big(1 + C_\Omega\|u\|^2_{L^\infty(0,T;W^{1,\infty}(\Omega))}\big)}\Big)\times \\
&\quad \times C\Big(\|e^1\|^2 + \|2e^1 - e^0\|^2 + \delta^4\tau^2 + \delta^4 + \tau^4\big(\|u_{tt}\|^2_{L^2(0,T;L^2(\Omega))} + \|u_{ttt}\|^2_{L^2(0,T;L^2(\Omega))}\big)\Big).
\end{aligned}$$

Proof. Taking the inner product of the momentum-error equation in (3.18) with τe^{n+1} followed by summation from $n = 1$ to $N - 1$ gives

$$\begin{aligned}
&\frac{1}{2}\|e^N\|^2 + \frac{1}{2}\|2e^N - e^{N-1}\|^2 + \frac{1}{2}\sum_{n=1}^{N-1}\|e^{n+1} - 2e^n + e^{n-1}\|^2 + \nu\tau\sum_{n=1}^{N-1}\|\nabla e^{n+1}\|^2 \\
&= \frac{1}{2}\|e^1\|^2 + \frac{1}{2}\|2e^1 - e^0\|^2 - \tau\sum_{n=1}^{N-1}\big((e^{n+1} \cdot \nabla)u(t^{n+1}), e^{n+1}\big) \\
&\quad - \tau\sum_{n=1}^{N-1}\big((u^{n+1} - 2u^n + u^{n-1}) \cdot \nabla)u(t^{n+1}), e^{n+1}\big) - \tau\sum_{n=1}^{N-1}\big((\varepsilon^{n+1} \cdot \nabla)u(t^{n+1}), e^{n+1}\big) \\
&\quad + \tau^2\sum_{n=1}^{N-1}\Big(\int_{t^{n-1}}^{t^{n+1}} K_1(t)\frac{\partial^3}{\partial t^3}u(t)\,dt, e^{n+1}\Big).
\end{aligned}$$

The trilinear forms are bounded above using Young's inequality, the Sobolev embeddings and the assumption of the regularity of the exact solution to the NSE equation, to obtain

$$\begin{aligned}
&-\big((e^{n+1} \cdot \nabla)u(t^{n+1}), e^{n+1}\big) - \big((u^{n+1} - 2u^n + u^{n-1}) \cdot \nabla)u(t^{n+1}), e^{n+1}\big) \\
&\qquad - \big((\varepsilon^{n+1} \cdot \nabla)u(t^{n+1}), e^{n+1}\big) \\
&\le \|\nabla u(t^{n+1})\|_{L^\infty(\Omega)}\|e^{n+1}\|^2 + \|\nabla u(t^{n+1})\|_{L^\infty(\Omega)}\|e^{n+1}\|\|u^{n+1} - 2u^n + u^{n-1}\|
\end{aligned}$$

$$+ \|\nabla u(t^{n+1})\|_{L^\infty(\Omega)}\|e^{n+1}\|\|\varepsilon^{n+1}\|$$
$$\leq C_\Omega \|u\|^2_{L^\infty(0,T;W^{1,\infty}(\Omega))}\|e^{n+1}\|^2 + \frac{1}{2}\|u^{n+1} - 2u^n + u^{n-1}\|^2 + \frac{1}{2}\|\varepsilon^{n+1}\|^2.$$

Therefore the above energy estimate for the errors writes

$$\frac{1}{2}\|e^N\|^2 + \frac{1}{2}\|2e^N - e^{N-1}\|^2 + \frac{1}{2}\sum_{n=1}^{N-1}\|e^{n+1} - 2e^n + e^{n-1}\|^2 + \nu\tau\sum_{n=1}^{N-1}\|\nabla e^{n+1}\|^2$$
$$\leq \frac{1}{2}\|e^1\|^2 + \frac{1}{2}\|2e^1 - e^0\|^2 + \tau\sum_{n=1}^{N-1} C_\Omega\|u\|^2_{L^\infty(0,T;W^{1,\infty}(\Omega))}\|e^{n+1}\|^2 + \tau\sum_{n=1}^{N-1}\frac{1}{2}\|\varepsilon^{n+1}\|^2$$
$$+ \tau\sum_{n=1}^{N-1}\frac{1}{2}\|u^{n+1} - 2u^n + u^{n-1}\|^2 + \tau\sum_{n=1}^{N-1}\|e^{n+1}\|^2 + C\tau^4\int_{t^0}^{t^N}\|u_{ttt}\|^2 dt.$$

Using now the second-order central finite difference approximation we have that the first term on the last line above can be bounded as

$$\frac{\tau}{2}\sum_{n=1}^{N-1}\|u^{n+1} - 2u^n + u^{n-1}\|^2 \leq \tau\sum_{n=1}^{N-1}\|e^{n+1} - 2e^n + e^{n-1}\|^2 + \tau^4\|u_{tt}\|^2_{L^2(0,T;L^2(\Omega))},$$

and therefore

$$\frac{1}{2}\|e^N\|^2 + \frac{1}{2}\|2e^N - e^{N-1}\|^2 + \Big(\frac{1}{2} - \tau\Big)\sum_{n=1}^{N-1}\|e^{n+1} - 2e^n + e^{n-1}\|^2 + \nu\tau\sum_{n=1}^{N-1}\|\nabla e^{n+1}\|^2$$
$$\leq \frac{1}{2}\|e^1\|^2 + \frac{1}{2}\|2e^1 - e^0\|^2 + \tau^4 C\big(\|u_{tt}\|^2_{L^2(0,T;L^2(\Omega))} + \|u_{ttt}\|^2_{L^2(0,T;L^2(\Omega))}\big)$$
$$+ \tau\sum_{n=1}^{N-1}\frac{1}{2}\|\varepsilon^{n+1}\|^2 + \big(1 + C_\Omega\|u\|^2_{L^\infty(0,T;W^{1,\infty}(\Omega))}\big)\tau\sum_{n=1}^{N-1}\|e^{n+1}\|^2.$$

We apply now Lemma 3.2 with $\phi^{n+1} \equiv w^{n+1} = 2u^n - u^{n-1}$. Note that in this case, the incompressibility condition (2.5) implies that the divergence terms in both (3.15) -(3.16) are nullified. Then the estimates (3.15) -(3.16) of the errors between the filtered and non-filtered values $\varepsilon^n = w^n - \overline{w^n}$ yield

$$\frac{1}{2}\|e^N\|^2 + \frac{1}{2}\|2e^N - e^{N-1}\|^2 + \Big(\frac{1}{2} - \tau\Big)\sum_{n=1}^{N-1}\|e^{n+1} - 2e^n + e^{n-1}\|^2 + \nu\tau\sum_{n=1}^{N-1}\|\nabla e^{n+1}\|^2$$
$$\leq \frac{1}{2}\|e^1\|^2 + \frac{1}{2}\|2e^1 - e^0\|^2 + \tau^4 C\big(\|u_{tt}\|^2_{L^2(0,T;L^2(\Omega))} + \|u_{ttt}\|^2_{L^2(0,T;L^2(\Omega))}\big)$$
$$+ C\big(\delta^4\tau^2 + \delta^4\big) + \big(1 + C_\Omega\|u\|^2_{L^\infty(0,T;W^{1,\infty}(\Omega))}\big)\tau\sum_{n=1}^{N-1}\|e^{n+1}\|^2.$$

The discrete Grönwall inequality [39, Lemma 5.1] completes the argument. ∎

3.3. Conditioning study. In this subsection, we will study the conditioning of the linear system arising from the spatial discretization of (2.3). To this end, we first recall a result from [27, Thm 1.1] about the solution of a linear system arising from solving an augmented Lagrangian system.

THEOREM 3.4. *Let $A \in \mathbb{R}^{n\times n}$ be an SPD matrix, $B \in \mathbb{R}^{m\times n}$ of* $\operatorname{rank}(B) = m$, *$f \in \mathbb{R}^n$, and $U \in \mathbb{R}^n$ solve*

$$\left(A + \frac{1}{\varepsilon}B^TB\right)U = -\frac{1}{\varepsilon}B^TBf.$$

If $\varepsilon < \frac{1}{\|S^{-1}\|}$, *where* $S = -BA^{-1}B^T$ *is the Schur complement matrix, then*

$$U = (C_0 + \varepsilon C_1)\, f, \quad C_0 = A^{-1}B^T S^{-1} B, C_1 = A^{-1}B^T S^{-1} \left(S - \varepsilon \mathrm{I}\right)^{-1} B,$$

where C_1 *is uniformly bounded with respect to* ε.

REMARK 3.5. *In the case of Stokes problem, the "pressure" operator* S *is a coercive, self-adjoint isomorphism of order zero.*

Now we state and prove the consequence of Theorem 3.4 on the condition number of our proposed filter (2.3) for the simplified case $a(\cdot) = 0$. The general case $a(\cdot) \neq 0$ is tested in the numerical experiments of Section 4.3.

COROLLARY 3.6. *Let* $A \in \mathbb{R}^{n\times n}$, *SPD matrix,* $B \in \mathbb{R}^{m\times n}$, $\mathrm{rank}(B) = m$, $f \in \mathbb{R}^n$, *and* $U \in \mathbb{R}^n$ *solve*

$$\left(A + \gamma B^T B\right) U = \left(A + \chi B^T B\right) f. \tag{3.19}$$

If $\gamma > \|S^{-1}\|$, *where* $S = -BA^{-1}B^T$ *is the Schur complement matrix, then*

$$U = f - \frac{\gamma - \chi}{\gamma}\left(C_0 + \frac{C_1}{\alpha}\right) f, \; C_0 = A^{-1}B^T S^{-1} B, C_1 = A^{-1}B^T S^{-1} \left(S - \frac{\mathrm{I}}{\gamma}\right)^{-1} B.$$

Proof. The conclusion directly follows from Theorem 3.4. Indeed, we rewrite (3.19) as

$$\left(A + \gamma B^T B\right) U = \left(A + \gamma B^T B - (\gamma - \chi) B^T B\right) f,$$

which immediately implies

$$U = f - \frac{\gamma - \chi}{\gamma}\left(A + \gamma B^T B\right)^{-1} \gamma B^T B f = f - \frac{\gamma - \chi}{\gamma}\left(C_0 + \frac{C_1}{\gamma}\right) f.$$

Thus, when $\gamma \gg 1$, the computational effort in solving (3.19) amounts to approximating the matrix $\mathrm{I} + C_0 - \frac{\chi}{\gamma} C_0$. ∎

4. Numerical Experiments. In this section we present several numerical experiments that test the features of our filtering scheme (2.3), and compare its performance against the "classical" adaptive filter (1.3). We used the $P_2 - P_1$ Taylor-Hood element pair [40] for the space approximations and direct solvers for solving the linear systems. All the tests below are performed using the FreeFem++ package [41].

4.1. Numerical testing of the filter (2.3). The goal in this subsection is to test the mass conservation accuracy and the damping of the high frequency modes of the solution. For simplicity, herein we consider the case of $a(\cdot) = 1$.

Test of accuracy: $\nabla \cdot w = 0$ case. The purpose of the first test is to verify the convergence rate of the proposed filter (2.3) when the source term is exactly div-free: $\nabla \cdot w = 0$. We consider

$$w_1 = \sin(\pi x)\cos(\pi y), \qquad w_2 = \cos(\pi x)\sin(\pi y)$$

in the unit square domain. The errors and the convergence rates of (2.3) are listed in Tables 4.1-4.2 for different values of γ and χ, all performed on uniform triangulations of the domain. It can be noted that the L_2 norm of divergence achieves a super-convergence of order 3, and a larger value of $\gamma - \chi$ improves its accuracy.

Test of accuracy: $\nabla \cdot w \simeq 0$ case. Next we report the filtering errors for the case of a weakly divergence-free source function w. Specifically, we compute the error when w is obtained by solving the Stokes equation on a unit square with the homogeneous Dirichlet boundary conditions.

The results reported in Table 4.3 confirm the predicted second order accuracy of the filter in both norms, although the L_2 norm achieves the second order accuracy only on finer meshes. The reason for this behavior is not clear, but we got very similar L_2 errors and rates with the filter (1.3) as well.

Table 4.1: Filtering errors when div$w = 0$, $\gamma = \chi = 1$ for (2.3), $e = \overline{w} - w$

h	$\|e\|$	rate	$\|\text{div}e\|$	rate
0.14142	0.166626	1.2655	0.00646797	2.9583
0.07071	0.0693071	1.6985	0.00083217	3.0842
0.03536	0.0213541	1.8823	9.81177e-5	3.0839
0.01778	0.00579233	1.9511	1.15714e-5	3.0511
0.00884	0.00149801	1.9782	1.39609e-6	3.0274
0.00442	0.000380199		1.71233e-7	

Table 4.2: Filtering errors when div$w = 0$, $\gamma - 1 = \chi = 1$ for (2.3), $e = \overline{w} - w$

h	$\|e\|$	rate	$\|\text{div}e\|$	rate
0.14142	0.166537	1.2649	0.00334046	2.9894
0.07071	0.0693019	1.6984	0.000420649	3.0902
0.03536	0.0213539	1.8823	4.93935e-5	3.0859
0.01778	0.00579233	1.9511	5.81734e-6	3.0519
0.00884	0.00149802	1.9782	7.01471e-7	3.0277
0.00442	0.00038021		8.60146e-8	

Table 4.3: Filtering errors when div$w = \mathcal{O}(h^2)$, $\gamma - 1 = \chi = 1$, $e = \overline{w} - w$

h	$\|e\|$	rate	$\|\text{div}e\|$	rate
0.14142	0.00127381	1.0448	0.0140668	1.9071
0.07071	0.000617447	1.3857	0.00375058	1.9393
0.03536	0.000236297	1.7065	0.000977965	2.0042
0.01778	7.24025e-5	1.8631	0.000243783	2.008
0.00884	1.99028e-5	1.9348	6.06088e-5	2.001
0.00442	5.20588e-6		1.51469e-5	

Test of scale damping. Here we test how well the proposed filter (2.3) damps a high wavenumber source function on an underresolved mesh. Specifically, we let

$$w_1 = \frac{\sin(40\pi x)\cos(40\pi y)}{40\pi}, \qquad w_2 = \frac{\cos(40\pi x)\sin(40\pi y)}{40\pi},$$

which is exactly div-free. Two different uniform meshes are considered with two different finite element spaces, as reported in the Table 4.4: Mesh 1 is the "Union Jack" type uniform mesh, while Mesh 2 is the default uniform mesh on FreeFem++. In the Table 4.4, m is the number of triangle edges on each side of the square. As can be observed, on a coarse mesh, the solution is completely filtered out.

4.2. Convergence Study. Next we present the convergence results with the manufactured solution

$$u_1 = \sin(2\pi x)\sin(2\pi(y+t)), \quad u_2 = \cos(2\pi x)\cos(2\pi(y+t)),$$
$$p = \cos(2\pi x)\sin(2\pi(y+t)), \quad f = u_t + u\cdot\nabla u - \nu\Delta u + \nabla p.$$

The domain is again taken to be a unit square and the final time is $T = 1$. We refine both the mesh size and the timestep τ, starting with $\tau = 0.01$. For simplicity, we take $\nu = 1$ and $a(u) = 1$.

Table 4.4: $\|\overline{w}\|_\infty$ on different meshes and with different polynomial spaces

m	(P_2, P_1) on Mesh 1	(P_2, P_1) on Mesh 2	Mini on Mesh 1	Mini on Mesh 2
10	7.31768e-17	7.97775e-17	5.87776e-17	8.03952e-17
20	1.80959e-16	1.01371e-16	2.77609e-16	3.82805e-16
21	0.0079355	0.0079355	0.0079355	0.0079355

We compare the accuracy of the Leray-α model of the classical nonlinear filter. The Table 4.5 and the Figure 4.1 confirm the expected convergence rates. Moreover, the levels of accuracy are comparable. It should be noted that, when testing the filter (1.3), we additionally included the grad-div stabilization term, as is usually done. This also increases the accuracy of the simulations.

Table 4.5: Errors in various norms with (2.3)

dt	$\|e^N\|$	$\|\nabla e\|_{l^2([0,T];L^2(\Omega))}$	$\|\nabla \cdot e^N\|$	$\|\nabla \cdot \overline{w^N}\|$
0.01	3.598101e-3	2.439480e-1	1.639737e-1	1.155800e-1
0.005	7.970590e-4	6.318691e-2	4.364989e-2	3.062503e-2
0.0025	2.150938e-4	1.718084e-2	1.111512e-2	7.886571e-3
0.00125	5.455494e-5	5.432974e-3	2.792415e-3	1.990771e-3

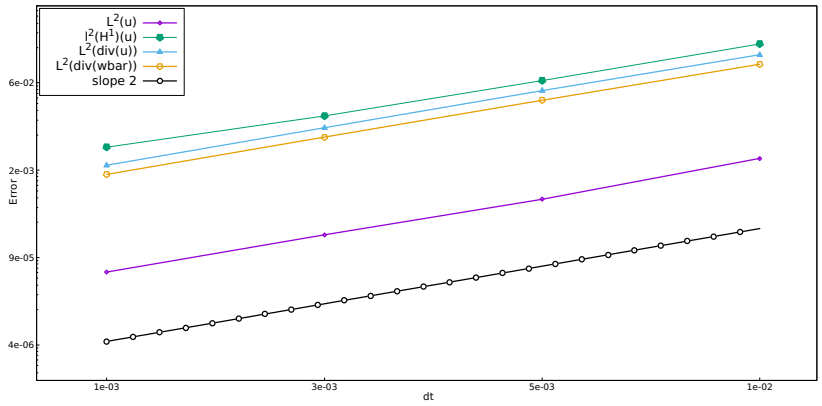

Fig. 4.1: Errors in logscale with the filter (2.3)

Table 4.6: Velocity errors in various norms with (1.3)

dt	$\|e^N\|$	$\|\nabla e\|_{l^2([0,T];L^2(\Omega))}$	$\|\nabla \cdot e^N\|$	$\|\nabla \cdot \overline{w^N}\|$
0.01	3.579735e-3	2.439955e-1	1.639683e-1	8.413938e-2
0.005	7.942565e-4	6.320913e-2	4.364966e-2	2.216186e-2
0.0025	2.154669e-4	1.718655e-2	1.111511e-2	5.812658e-3
0.00125	5.481368e-5	5.434031e-3	2.792414e-3	1.484879e-3

4.3. Condition number study. We study the dependence on the parameters γ and χ of the condition number κ of the linear system arising from the space discretization of (2.3), for various meshes and domains. Suppose that

$$X_h := \text{span}\{\phi_1, ..., \phi_n\} \subset C^0(\Omega) \cap H_0^1(\Omega)$$

is the standard finite element space of degree 2. Letting

$$\begin{aligned} M_{\gamma,ij} :=& \delta^2 (\nabla\phi_i, \nabla\phi_j) + (\phi_i, \phi_j)_{\mathrm{H}_{\gamma,\mathrm{div}}}, 1 \le i,j \le n \\ M_{\chi,ij} :=& \delta^2 ((1-a)\nabla\phi_i, \nabla\phi_j) + (\phi_i, \phi_j)_{\mathrm{H}_{\chi,\mathrm{div}}}, 1 \le i,j \le n \\ M :=& M_\gamma^{-1} M_\chi, \end{aligned}$$

we explicitly compute the condition number $\kappa(M)$ of the matrix M. The indicator function $a(\cdot)$ is taken to be a P_1 finite element function that assigns random values between 0 and 1 at each degree of freedom.

First we evaluate $\kappa(M)$ on the unit square domain with a uniform triangulation. As can be seen from Tables 4.7-4.9, for fixed γ and χ, $\kappa(M)$ exhibits negligible changes with respect to the meshsize h. On the other hand, a fixed mesh size and "smaller" values of γ/χ give an almost uniform condition number. However, already at $\gamma/\chi \simeq 10$, the condition number is effectively given by γ/χ, suggesting that the result of Theorem 3.6 is true even for the $a(\cdot) \neq 0$ case.

We also compute $\kappa(M)$ on the complex domain around the NACA0012 airfoil, shown in Figure 4.2, on a family of non-uniform meshes. The results, not as extensive as the square domain case, are given in Table 4.10. As in the previous case, a very weak dependence on the meshsize h and the estimate $\kappa(M) \simeq \gamma/\chi$ can be observed.

h \ γ,χ	$\gamma=2,\chi=1$	$\gamma=20,\chi=10$	$\gamma=200,\chi=100$	$\gamma=2000,\chi=1000$
$\frac{1}{10}$	4.29082	3.77587	3.64373	3.62588
$\frac{1}{20}$	5.53434	5.19076	5.14633	5.14132
$\frac{1}{40}$	6.09946	5.90711	5.86958	5.86379
$\frac{1}{60}$	7.88369	7.83545	7.8297	7.8291
$\frac{1}{80}$	8.00806	7.97113	7.96622	7.96563

Table 4.7: Condition numbers: Uniform mesh on square domain, $\gamma/\chi = 2$

h \ γ,χ	$\gamma=5,\chi=1$	$\gamma=50,\chi=10$	$\gamma=500,\chi=100$	$\gamma=5000,\chi=1000$
$\frac{1}{10}$	5.09409	5.01164	5.00119	5.00012
$\frac{1}{20}$	6.1747	5.45287	5.21366	5.00695
$\frac{1}{40}$	6.38406	5.98769	5.88614	5.01838
$\frac{1}{60}$	7.93104	7.84178	7.83041	7.82917
$\frac{1}{80}$	8.04244	7.97593	7.96685	7.9657

Table 4.8: Condition numbers: Uniform mesh on square domain, $\gamma/\chi = 5$

h \ γ, χ	$\gamma = 10, \chi = 1$	$\gamma = 100, \chi = 10$	$\gamma = 1000, \chi = 100$	$\gamma = 10000, \chi = 1000$
$\frac{1}{10}$	9.99981	9.99981	9.99981	9.99981
$\frac{1}{20}$	10.001	10	10	10
$\frac{1}{40}$	10	10	10	10
$\frac{1}{60}$	10	10	10	10
$\frac{1}{80}$	10	10	10.0001	10.0001

Table 4.9: Condition numbers: Uniform mesh on square domain, $\gamma/\chi = 10$

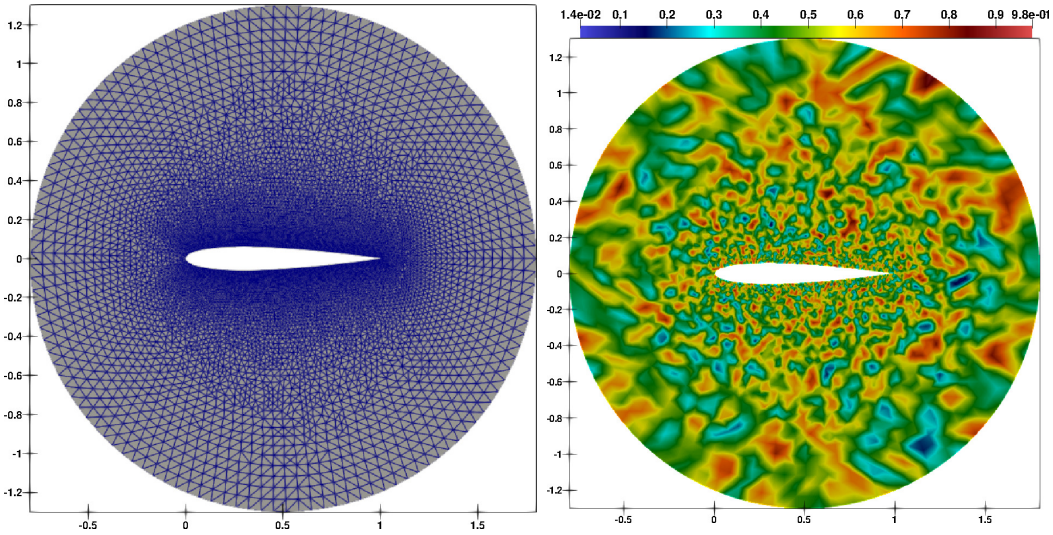

Fig. 4.2: NACA0012 airfoild domain mesh (left) and a random $a(\cdot)$ field (right)

h \ γ, χ	$\gamma = 2, \chi = 1$	$\gamma = 2000, \chi = 1000$	$\gamma = 5, \chi = 1$	$\gamma = 5000, \chi = 1000$
$[0.017, 0.22]$	6.39783	6.39125	6.411	5.00102
$[0.012, 0.157]$	9.62535	9.59801	9.64161	5.00141
$[0.008, 0.112]$	7.92431	7.91915	7.92952	5.00136
$[0.0064, 0.09]$	8.8414	8.75797	8.8971	5.00072

Table 4.10: Condition numbers: NACA0012 airfoil domain

4.4. 2D Kelvin-Helmholtz instability. In this subsection we compare the performance of the Leray-α model with both filters (2.3) and (1.3), on the two dimensional mixing layer problem from [42] (https://ngsolve.org/showcases/kh-benchmark). Better known as the Kelvin-Helmholtz instability problem, it has been used as a test problem by many authors, e.g. [43, 44, 45, 46]. The problem's physical domain is taken to be the unit square $\Omega = (0, 1)^2$. The boundary conditions are

At x-boundary: Periodic

$$u(0,y) = u(1,y)$$

At y-boundary: No penetration and free-slip

$$u \cdot \mathbf{n} = 0,$$
$$(-\nu \nabla u \cdot \mathbf{n}) \times \mathbf{n} = 0.$$

For the filtering step (2.3), the boundary conditions at the x boundaries are periodic

$$\overline{w^{n+1}}(0,y) = \overline{w^{n+1}}(1,y),$$

while at the y-boundary, we impose

$$\begin{aligned} &\overline{w}^{n+1} \cdot \mathbf{n} = 0, \\ &\Big[-\delta^2 \nabla \Big(\overline{w^{n+1}} - \big(1 - a(w^{n+1})\big)\overline{w^n} \Big) \cdot \mathbf{n} - \nabla \cdot (w^{n+1} - \overline{w^{n+1}})\mathbf{n} \Big] \times \mathbf{n} = 0. \end{aligned} \tag{4.1}$$

The above boundary condition (4.1) sets the tangential component of the "filter stress" tensor equal to zero. A similar "free-slip" condition is used for the (1.3) filter. In (4.1), the indicator function from (2.1) is used.

The initial condition is given by

$$\begin{aligned} u_0 &= \begin{bmatrix} u_\infty \tanh\left((2y-1)/\delta_0\right) \\ 0 \end{bmatrix} + 10^{-3} \begin{bmatrix} \partial_y \psi(x,y) \\ -\partial_x \psi(x,y) \end{bmatrix}, \\ \psi(x,y) &= \exp\Big(-\frac{(y-0.5)^2}{\delta_0^2} \Big) \left[\cos(8\pi x) + \cos(20\pi x) \right]. \end{aligned} \tag{4.2}$$

We consider the case with the initial vorticity thickness $\delta_0 = 1/28$, the reference velocity $u_\infty = 1$, and the Reynolds number $\mathrm{Re} = u_\infty \delta_0 / \nu = 10^4$. The results are reported at non-dimensional time units $\bar{t} = \delta_0 / u_\infty$.

We tested the schemes on various meshes and with different time steps. Herein, we report the results for $\tau = 1e-3$ and a 48×48 uniform triangular mesh. The simulations are run until $\bar{t} \leq 400$. In Figures 4.3-4.6 we refer to the results of our Algorithm 2.1 as "Leray 1", while the results obtained with the filter (1.3) are labelled as "Leray 2".

The expected behavior of the flow is as follows. Through the action of the nonlinear term, the perturbations in the initial condition (4.2) are amplified and four vortices develop around $y = 0.5$ line. Later on, the first vortex merges with the second one, while the third vortex merges with the fourth. After a while, those two merge into a single vortex around the origin. The accurate prediction of the pairing time of the last two vortices is known to be very challenging, and vastly different merging times have been reported in the literature (a different merging pattern has been reported in [47]). The underlying reason for this discrepancy is the extreme sensitivity of the Kelvin-Helmholtz problem to various perturbations, as has been thoroughly tested and documented in [42]. Besides being sensitive to inevitable discretization errors, it has been shown to be sensitive to the mesh types (triangular versus quadrilateral, structured vs. unstructured), linear solvers and quadrature rules and even compiler settings. As a result, the mesh convergence has been obtained only for $\bar{t} < 200$, even on a 256×256 grid with H(div) conforming 8-th degree DG scheme, and a timestep of $\tau = 3.6 \times 10^{-5}$. Thus, even though we report our findings for $\bar{t} \leq 400$, it makes sense to compare them only for $\bar{t} < 200$. We shall refer to the results of [42] as DNS in the following discussion.

Kinetic energy. The evolution of the kinetic energy $\dfrac{\|u\|^2}{2}$ is plotted in Figure 4.3. The energy is expected to decrease monotonically with time, both for the Navier-Stokes system and the Leray model, regardless of the filtering used. This is clearly observed in both cases, and moreover, the kinetic energies are almost identical.

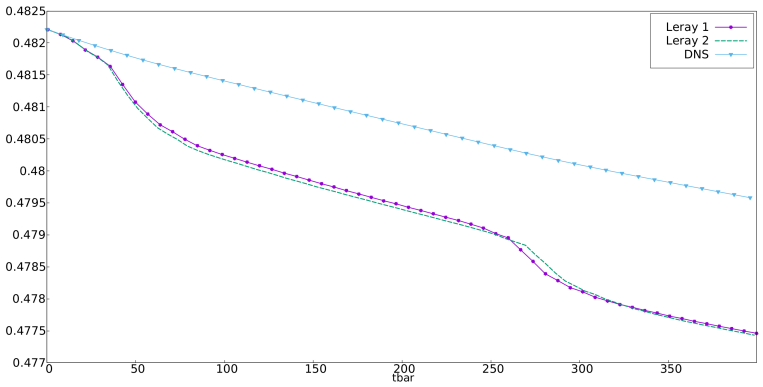

Fig. 4.3: Kinetic energy

Enstrophy. The evolution of the enstrophy $\frac{\|\nabla \times u\|^2}{2}$ is plotted in Figure 4.4. Enstrophy is also a monotonically decreasing quantity for the Navier-Stokes system. However, that is not necessarily true for the Leray model. In fact, according to [48], for the case of a fully periodic domain with linear Helmholtz filter (1.2), a modified enstrophy

$$\frac{\|\nabla \times \overline{u}\|^2}{2} + \delta^2 \frac{\|\Delta \overline{u}\|^2}{2}$$

is a decreasing quantity. This is most probably not true for any of the nonlinear filters.

Comparing the graphs of both cases, we see that they agree up to the time $\bar{t} \simeq 240$, after which there seems to be a phase difference for some time. Again, this difference at around $\bar{t} \simeq 250$ could be attributed to many factors, such as the problem itself being very sensitivity to any perturbations, and/or due to the time relaxation [49] introduced by the Voigt regularization term in (2.3).

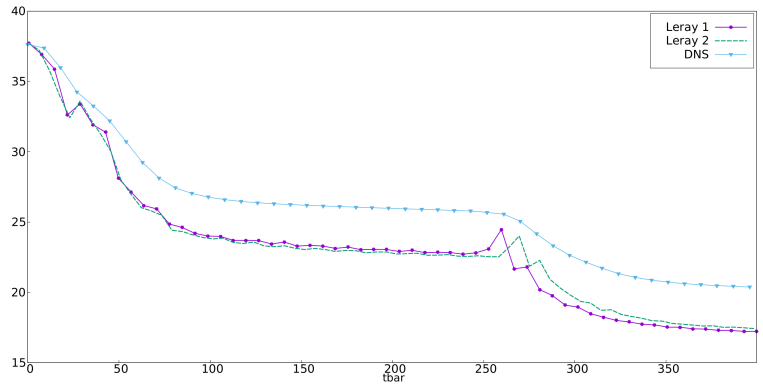

Fig. 4.4: Enstrophy

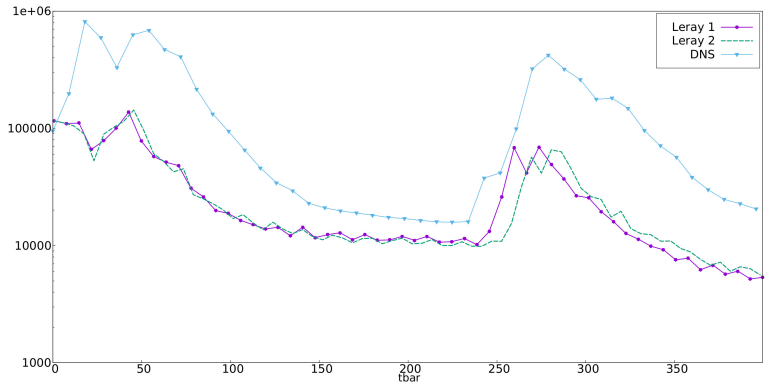

Fig. 4.5: Palinstrophy

Palinstrophy. The evolution of palinstrophy $\frac{\|\nabla(\nabla\times u)\|^2}{2}$ is plotted in Figure 4.5. For the velocity-pressure formulation of the Navier-Stokes equation, palinstrophy is the most challenging quantity to predict, as there is no control over its accuracy. Overall, we see that the results follow the trend of the DNS solution, and a difference at around $\bar{t} \simeq 250$ is again observed. The spontaneous increases in palinstrophy usually correspond to merging of the vortices. Looking at the Figure 4.5, the outburst in both graphs occur at around $\bar{t} \simeq 250$, which is close to the predictions of the DNS study [42]. Most reported results predict much earlier pairing time for the last two vortices.

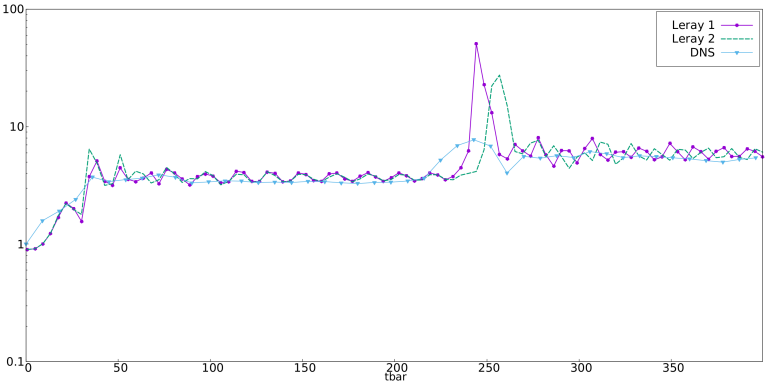

Fig. 4.6: Relative vorticity thickness

Vorticity thickness. The evolution of the relative vorticity thickness

$$\delta(t) = \frac{2u_\infty}{\sup\limits_{y\in[0,1]} |<\chi>(t,y)|}, \quad <\chi>(t,y) = \int_0^1 \chi(t,x,y)dx$$

is plotted in Figure 4.5. The oscillatory behavior of $\delta(t)$ indicates that the vortices are ellipsoidal, while its smoothness means they are of circular shape. A very similar trend to the earlier graphs is again observed.

Finally, the qualitative results in terms of vorticity contours are reported in Figures 4.7 and 4.8. The plots look similar up to $\bar{t} < 200$, and some differences can be observed at later times.

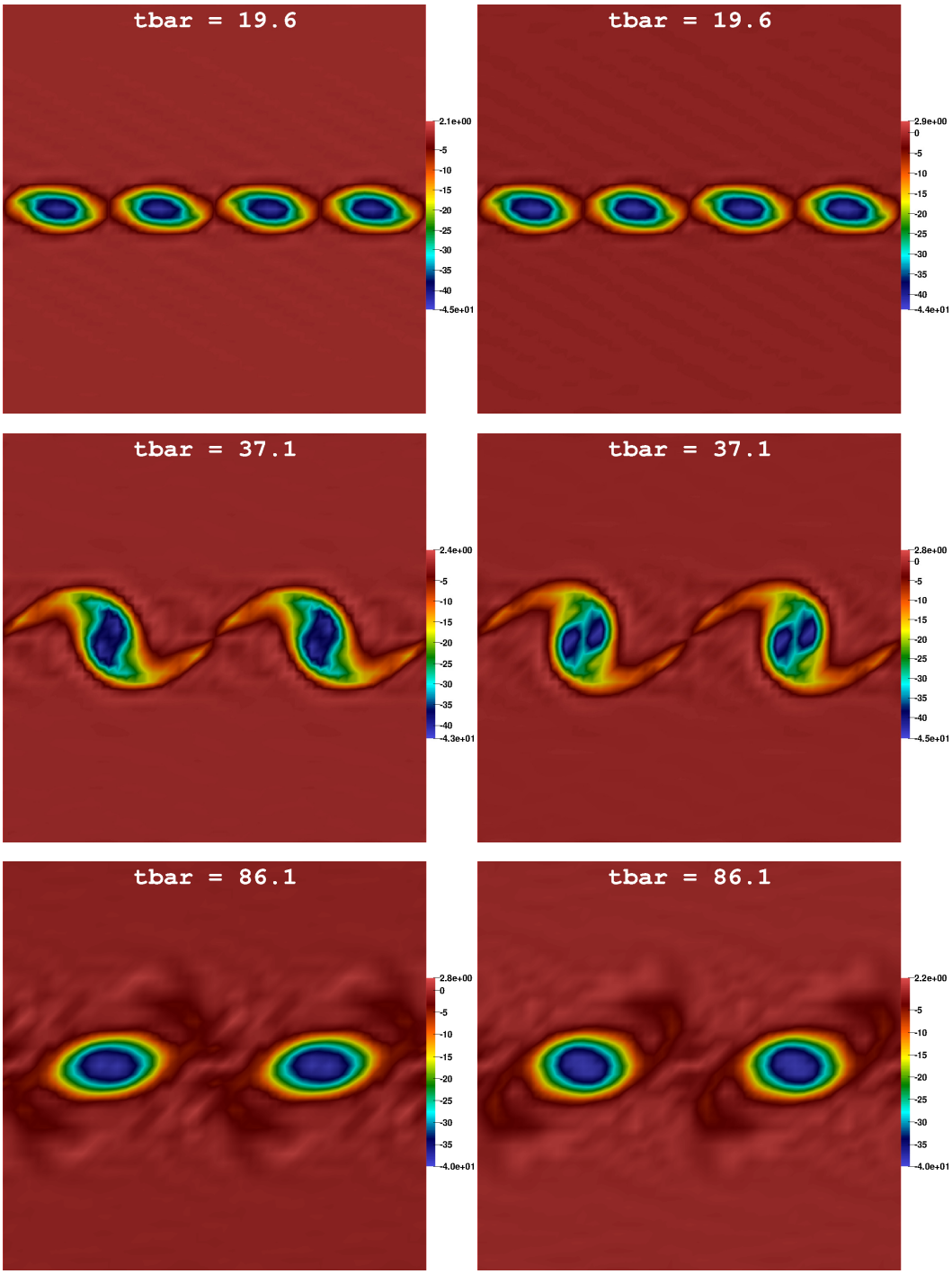

Fig. 4.7: Vorticity contours at various times: New filter (left) and old filter (right)

5. Conclusions. We propose a nonlinear filtering operator, which adapts both in space and in time to the flow patterns. The novelty consists in its reduced computational cost: the new filter requires a single matrix assembly throughout the numerical integration, and the solution of a constant coefficient elliptic problem at each time step. We proved the filter's stability and second-order accuracy. Then we discussed its synthesis with the Leray-α model,

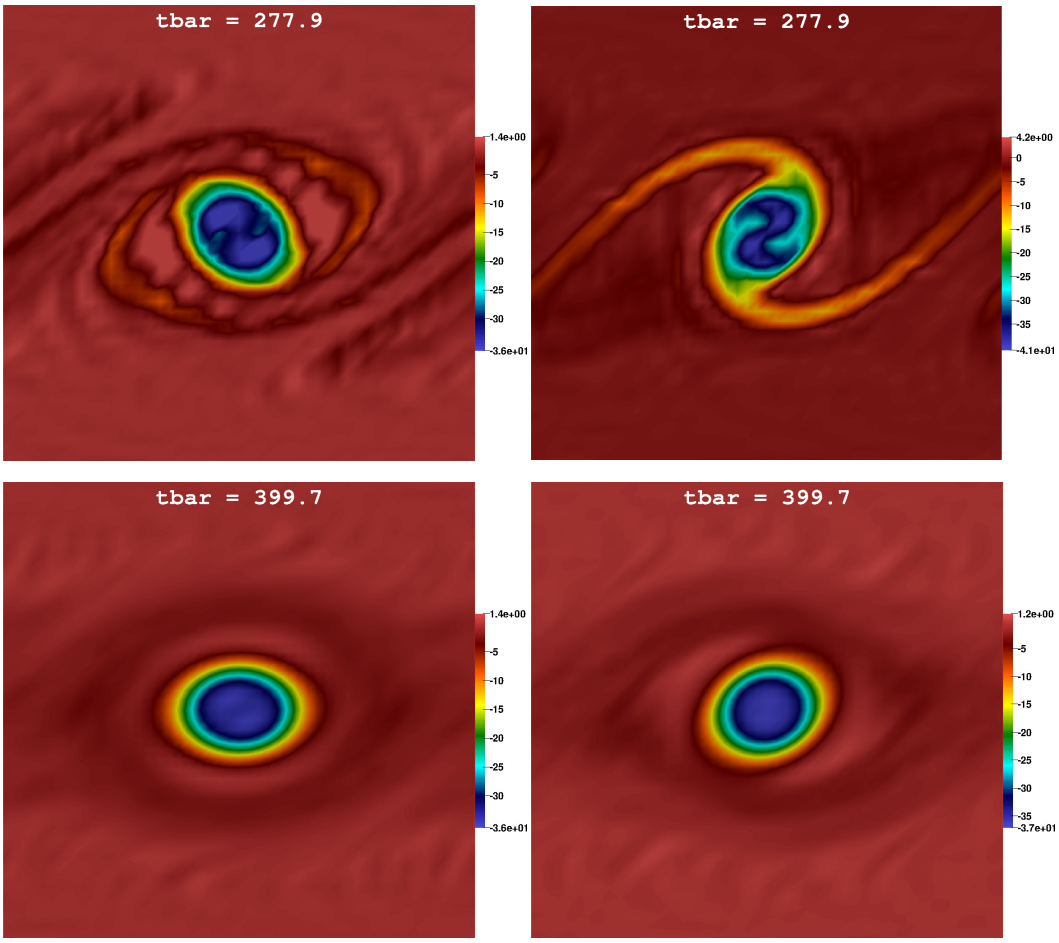

Fig. 4.8: Vorticity contours at various times: New filter (left) and old filter (right)

and established its analytical foundations. While the numerical tests demonstrate that the new filter (2.3) and old filter (1.3) have the same level of accuracy, the computational gains from using (2.3) could be significant.

6. Acknowledgements. The first author would like to acknowledge the support, under a Seed Research Project no. 21021440101, of University of Sharjah.

The authors would like to acknowledge very helpful discussions with Dr. John Burkardt (University of Pittsburgh).

REFERENCES

[1] V. John, Large eddy simulation of turbulent incompressible flows, Vol. 34 of Lecture Notes in Computational Science and Engineering, Springer-Verlag, Berlin, 2004, analytical and numerical results for a class of LES models.

[2] M. Lesieur, O. Metais, P. Comte, Large-eddy simulations of turbulence, Cambridge University Press, New York, 2005, with a preface by James J. Riley. doi:10.1017/CBO9780511755507. URL https://doi-org.pitt.idm.oclc.org/10.1017/CBO9780511755507

[3] L. C. Berselli, T. Iliescu, W. J. Layton, Mathematics of large eddy simulation of turbulent flows, Scientific Computation, Springer-Verlag, Berlin, 2006.

[4] P. Sagaut, Large eddy simulation for incompressible flows, 3rd Edition, Scientific Computation, Springer-Verlag, Berlin, 2006, an introduction, Translated from the 1998 French original, With forewords by Marcel Lesieur and Massimo Germano, With a foreword by Charles Meneveau.

[5] B. J. Geurts, Direct and Large-Eddy Simulation, De Gruyter, 2022.

[6] M. Germano, Differential filters for the large eddy numerical simulation of turbulent flows, Phys. Fluids 29 (6) (1986) 1755–1757. doi:10.1063/1.865649.
URL https://doi-org.pitt.idm.oclc.org/10.1063/1.865649

[7] B. J. Geurts, D. D. Holm, Regularization modeling for large-eddy simulation, Phys. Fluids 15 (1) (2003) L13–L16. doi:10.1063/1.1529180.
URL https://doi-org.pitt.idm.oclc.org/10.1063/1.1529180

[8] B. J. Geurts, D. D. Holm, Leray and LANS-α modelling of turbulent mixing, J. Turbul. 7 (2006) Paper 10, 33. doi:10.1080/14685240500501601.
URL https://doi-org.pitt.idm.oclc.org/10.1080/14685240500501601

[9] W. Layton, C. C. Manica, M. Neda, L. G. Rebholz, Numerical analysis and computational testing of a high accuracy leray-deconvolution model of turbulence, Numerical Methods for Partial Differential Equations 24 (2) (2008) 555–582. arXiv:https://onlinelibrary.wiley.com/doi/pdf/10.1002/num.20281, doi:https://doi.org/10.1002/num.20281.
URL https://onlinelibrary.wiley.com/doi/abs/10.1002/num.20281

[10] W. Layton, L. G. Rebholz, C. Trenchea, Modular nonlinear filter stabilization of methods for higher Reynolds numbers flow, J. Math. Fluid Mech. 14 (2) (2012) 325–354. doi:10.1007/s00021-011-0072-z.
URL http://dx.doi.org/10.1007/s00021-011-0072-z

[11] W. Layton, N. Mays, M. Neda, C. Trenchea, Numerical analysis of modular regularization methods for the BDF2 time discretization of the Navier-Stokes equations, ESAIM Math. Model. Numer. Anal. 48 (3) (2014) 765–793. doi:10.1051/m2an/2013120.
URL https://doi-org.pitt.idm.oclc.org/10.1051/m2an/2013120

[12] A. L. Bowers, L. G. Rebholz, A. Takhirov, C. Trenchea, Improved accuracy in regularization models of incompressible flow via adaptive nonlinear filtering, Internat. J. Numer. Methods Fluids 70 (7) (2012) 805–828. doi:10.1002/fld.2732.
URL https://doi-org.pitt.idm.oclc.org/10.1002/fld.2732

[13] A. L. Bowers, L. G. Rebholz, Numerical study of a regularization model for incompressible flow with deconvolution-based adaptive nonlinear filtering, Comput. Methods Appl. Mech. Engrg. 258 (2013) 1–12. doi:10.1016/j.cma.2013.02.003.
URL https://doi-org.pitt.idm.oclc.org/10.1016/j.cma.2013.02.003

[14] L. Bertagna, A. Quaini, A. Veneziani, Deconvolution-based nonlinear filtering for incompressible flows at moderately large Reynolds numbers, Internat. J. Numer. Methods Fluids 81 (8) (2016) 463–488. doi:10.1002/fld.4192.
URL https://doi-org.pitt.idm.oclc.org/10.1002/fld.4192

[15] A. Takhirov, A. Lozovskiy, Computationally efficient modular nonlinear filter stabilization for high Reynolds number flows, Adv. Comput. Math. 44 (1) (2018) 295–325. doi:10.1007/s10444-017-9544-x.
URL https://doi-org.pitt.idm.oclc.org/10.1007/s10444-017-9544-x

[16] A. Takhirov, C. Trenchea, J. Waters, Second-order efficient nonlinear filter stabilization for high Reynolds number flows, Numerical Methods for Partial Differential Equations (2021).
URL https://doi.org/10.1002/num.22859

[17] J. Leray, Sur le mouvement d'un liquide visqueux emplissant l'espace, Acta Math. 63 (1) (1934) 193–248. doi:10.1007/BF02547354.
URL https://doi-org.pitt.idm.oclc.org/10.1007/BF02547354

[18] A. Cheskidov, D. D. Holm, E. Olson, E. S. Titi, On a Leray-alpha model of turbulence, Proceedings of the Royal Society A: Mathematical, Physical and Engineering Sciences 461 (2055) (2005) 629–649. arXiv:https://royalsocietypublishing.org/doi/pdf/10.1098/rspa.2004.1373, doi:10.1098/rspa.2004.1373.
URL https://royalsocietypublishing.org/doi/abs/10.1098/rspa.2004.1373

[19] S. Stolz, N. A. Adams, An approximate deconvolution procedure for large-eddy simulation, Physics of Fluids 11 (7) (1999) 1699–1701. arXiv:https://doi.org/10.1063/1.869867, doi:10.1063/1.869867.
URL https://doi.org/10.1063/1.869867

[20] J. Bardina, J. H. Ferziger, W. C. Reynolds, Improved subgrid-scale models for large-eddy simulation, AIAA 13th Fluid & Plasma Dynamics Conference, 1980. arXiv:https://arc.aiaa.org/doi/pdf/10.2514/6.1980-1357, doi:10.2514/6.1980-1357.
URL https://arc.aiaa.org/doi/abs/10.2514/6.1980-1357

[21] M. van Reeuwijk, H. J. Jonker, K. Hanjalic, Leray-alpha simulations of wall-bounded turbulent flows, International Journal of Heat and Fluid Flow 30 (6) (2009) 1044–1053. doi:https://doi.org/10.1016/j.ijheatfluidflow.2009.08.001.
URL https://www.sciencedirect.com/science/article/pii/S0142727X09001210

[22] F. Picano, K. Hanjalić, Leray-alpha regularization of the Smagorinsky-closed filtered equations for turbulent jets at high Reynolds numbers, Flow Turbulence and Combustion 89 (2012) 627–650.

[23] J.-L. Guermond, On the use of the notion of suitable weak solutions in CFD, Internat. J. Numer. Methods Fluids 57 (9) (2008) 1153–1170. doi:10.1002/fld.1853.
URL https://doi-org.pitt.idm.oclc.org/10.1002/fld.1853

[24] J.-L. Guermond, R. Pasquetti, B. Popov, From suitable weak solutions to entropy viscosity, J. Sci. Comput. 49 (1) (2011) 35–50. doi:10.1007/s10915-010-9445-3.

URL https://doi-org.pitt.idm.oclc.org/10.1007/s10915-010-9445-3
[25] J.-L. Guermond, P. D. Minev, High-order time stepping for the Navier-Stokes equations with minimal computational complexity, J. Comput. Appl. Math. 310 (2017) 92–103. doi:10.1016/j.cam.2016.04.033.
URL https://doi-org.pitt.idm.oclc.org/10.1016/j.cam.2016.04.033
[26] J.-L. Guermond, P. Minev, High-order time stepping for the incompressible Navier-Stokes equations, SIAM J. Sci. Comput. 37 (6) (2015) A2656–A2681. doi:10.1137/140975231.
URL https://doi-org.pitt.idm.oclc.org/10.1137/140975231
[27] P. Angot, J.-P. Caltagirone, P. Fabrie, A new fast method to compute saddle-points in constrained optimization and applications, Appl. Math. Lett. 25 (3) (2012) 245–251. doi:10.1016/j.aml.2011.08.015.
URL https://doi-org.pitt.idm.oclc.org/10.1016/j.aml.2011.08.015
[28] P. Angot, R. Cheaytou, On the error estimates of the vector penalty-projection methods: second-order scheme, Math. Comp. 87 (313) (2018) 2159–2187. doi:10.1090/mcom/3309.
URL https://doi-org.pitt.idm.oclc.org/10.1090/mcom/3309
[29] D. F. Griffiths, J. M. Sanz-Serna, On the scope of the method of modified equations, SIAM J. Sci. Statist. Comput. 7 (3) (1986) 994–1008. doi:10.1137/0907067.
URL http://dx.doi.org/10.1137/0907067
[30] D. F. Griffiths, D. J. Higham, Numerical methods for ordinary differential equations, Springer Undergraduate Mathematics Series, Springer-Verlag London, Ltd., London, 2010, initial value problems. doi:10.1007/978-0-85729-148-6.
URL http://dx.doi.org/10.1007/978-0-85729-148-6
[31] E. Hairer, C. Lubich, G. Wanner, Geometric numerical integration, Vol. 31 of Springer Series in Computational Mathematics, Springer, Heidelberg, 2010, structure-preserving algorithms for ordinary differential equations, Reprint of the second (2006) edition.
[32] R. D. Ruth, A canonical integration technique, IEEE Trans. Nucl. Sci (1983) 2669–2671.
[33] A. Guzel, C. Trenchea, The Williams step increases the stability and accuracy of the hoRA time filter, Appl. Numer. Math. 131 (2018) 158–173. doi:10.1016/j.apnum.2018.05.003.
URL https://doi-org.pitt.idm.oclc.org/10.1016/j.apnum.2018.05.003
[34] M. Bukač, C. Trenchea, Boundary update via resolvent for fluid–structure interaction, J. Numer. Math. 29 (1) (2021) 1–22. doi:10.1515/jnma-2019-0081.
URL https://doi-org.pitt.idm.oclc.org/10.1515/jnma-2019-0081
[35] H. Brezis, Functional analysis, Sobolev spaces and partial differential equations, Universitext, Springer, New York, 2011.
[36] E. Hairer, G. Wanner, Solving ordinary differential equations. II, Vol. 14 of Springer Series in Computational Mathematics, Springer-Verlag, Berlin, 2010, stiff and differential-algebraic problems, Second revised edition. doi:10.1007/978-3-642-05221-7.
URL http://dx.doi.org/10.1007/978-3-642-05221-7
[37] M. R. Garvie, C. Trenchea, A three level finite element approximation of a pattern formation model in developmental biology, Numer. Math. 127 (3) (2014) 397–422. doi:10.1007/s00211-013-0591-z.
URL http://dx.doi.org.pitt.idm.oclc.org/10.1007/s00211-013-0591-z
[38] W. Layton, C. Trenchea, Stability of two IMEX methods, CNLF and BDF2-AB2, for uncoupling systems of evolution equations, Appl. Numer. Math. 62 (2) (2012) 112–120. doi:10.1016/j.apnum.2011.10.006.
URL http://dx.doi.org.pitt.idm.oclc.org/10.1016/j.apnum.2011.10.006
[39] J. G. Heywood, R. Rannacher, Finite-element approximation of the nonstationary Navier-Stokes problem. IV. Error analysis for second-order time discretization, SIAM J. Numer. Anal. 27 (2) (1990) 353–384. doi:10.1137/0727022.
URL http://dx.doi.org/10.1137/0727022
[40] D. N. Arnold, J. Qin, Quadratic velocity/linear pressure Stokes elements, in: R. Vichnevetsky, D. Knight, G. Richter (Eds.), Advances in Computer Methods for Partial Differential Equations VII, IMACS, 1992, pp. 28–34.
[41] F. Hecht, New development in FreeFem++, J. Numer. Math. 20 (3-4) (2012) 251–265.
[42] P. W. Schroeder, V. John, P. L. Lederer, C. Lehrenfeld, G. Lube, J. Schöberl, On reference solutions and the sensitivity of the 2D Kelvin-Helmholtz instability problem, Comput. Math. Appl. 77 (4) (2019) 1010–1028. doi:10.1016/j.camwa.2018.10.030.
URL https://doi-org.pitt.idm.oclc.org/10.1016/j.camwa.2018.10.030
[43] V. Gravemeier, W. A. Wall, E. Ramm, Large eddy simulation of turbulent incompressible flows by a three-level finite element method, International Journal for Numerical Methods in Fluids 48 (10) (2005) 1067–1099. arXiv:https://onlinelibrary.wiley.com/doi/pdf/10.1002/fld.961, doi:https://doi.org/10.1002/fld.961.
URL https://onlinelibrary.wiley.com/doi/abs/10.1002/fld.961
[44] M. Lesieur, C. Staquet, P. Le Roy, P. Comte, The mixing layer and its coherence examined from the point of view of two-dimensional turbulence, J. Fluid Mech. 192 (1988) 511–534. doi:10.1017/S002211208800196X.
URL https://doi-org.pitt.idm.oclc.org/10.1017/S002211208800196X
[45] V. John, An assessment of two models for the subgrid scale tensor in the rational LES model, Journal of Computational and Applied Mathematics 173 (1) (2005) 57–80. doi:https://doi.org/10.1016/

j.cam.2004.02.022.
URL https://www.sciencedirect.com/science/article/pii/S0377042704001347

[46] N. Ahmed, T. Chacón Rebollo, V. John, S. Rubino, Analysis of a full space-time discretization of the Navier-Stokes equations by a local projection stabilization method, IMA J. Numer. Anal. 37 (3) (2017) 1437–1467. doi:10.1093/imanum/drw048.
URL https://doi-org.pitt.idm.oclc.org/10.1093/imanum/drw048

[47] L. G. Rebholz, D. Vargun, M. Xiao, Enabling convergence of the iterated penalty Picard iteration with $O(1)$ penalty parameter for incompressible Navier-Stokes via Anderson acceleration, Comput. Methods Appl. Mech. Engrg. 387 (2021) Paper No. 114178, 17. doi:10.1016/j.cma.2021.114178.
URL https://doi-org.pitt.idm.oclc.org/10.1016/j.cma.2021.114178

[48] L. G. Rebholz, Conservation laws of turbulence models, Journal of Mathematical Analysis and Applications 326 (1) (2007) 33–45. doi:https://doi.org/10.1016/j.jmaa.2006.02.026.
URL https://www.sciencedirect.com/science/article/pii/S0022247X06001399

[49] A. Takhirov, Voigt regularization for the explicit time stepping of the Hall effect term, Geophys. Astrophys. Fluid Dyn. 110 (5) (2016) 409–431. doi:10.1080/03091929.2016.1195376.
URL https://doi-org.pitt.idm.oclc.org/10.1080/03091929.2016.1195376